Interannual and Decadal Variations in Cross-Shelf Transport in the Gulf of Alaska

VINCENT COMBES AND EMANUELE DI LORENZO

School of Earth and Atmospheric Sciences, Georgia Institute of Technology, Atlanta, Georgia

ENRIQUE CURCHITSER

Institute of Marine and Coastal Sciences, Rutgers, The State University of New Jersey, New Brunswick, New Jersey

(Manuscript received 12 March 2008, in final form 12 November 2008)

ABSTRACT

The marine ecosystem of the Gulf of Alaska (GOA) is one of the richest on the planet. The center of the GOA is characterized by high-nutrient and low-chlorophyll-*a* concentration. Recent observational studies suggest that advection of iron-rich coastal water is the primary mechanism controlling open ocean productivity. Specifically, there is evidence that mesoscale eddies along the coastal GOA entrain iron-rich coastal waters into the ocean interior. This study investigates the cross-shelf transport statistics in the GOA using a free-surface, hydrostatic, eddy-resolving primitive equation model over the period 1965–2004. The statistics of coastal water transport are computed using a model passive tracer, which is continuously released at the coast. The passive tracer can thus be considered a proxy for coastal biogeochemical quantities such as silicate, nitrate, iron, or oxygen, which are critical for explaining the GOA ecosystem dynamics. On average along the Alaska Current, it has been shown that at the surface while the advection of tracers by the average flow is directed toward the coast consistent with the dominant downwelling regime of the GOA, it is the mean eddy fluxes that contribute to offshore advection into the gyre interior. South of the Alaskan Peninsula, both the advection of tracers by the average flow and the mean eddy fluxes contribute to the mean offshore advection. On interannual and longer time scales, the offshore transport of the passive tracer in the Alaskan Stream does not correlate with large-scale atmospheric forcing, nor with local winds. In contrast in the Alaska Current region, stronger offshore transport of the passive tracer coincides with periods of stronger downwelling (in particular during positive phases of the Pacific decadal oscillation), which trigger the development of stronger eddies.

1. Introduction

The waters of the Gulf of Alaska (GOA) and the Bering Sea provide more than half of the total annual fish catch for the United States. The central Gulf of Alaska reveals a high-nutrient/low-chlorophyll (HNLC) region with iron limitation (Harrison et al. 1999; Boyd et al. 2004). There is evidence that eddies, generated at the coast, impact iron distribution and therefore play a role in maintaining high-chlorophyll concentration. The mesoscale eddies generated along the Alaska Current (eastern basin) transport nutrients (Whitney and Robert 2002; Ladd et al. 2005) and iron (Johnson et al. 2005) to the interior. More specifically, Batten and Crawford (2005) observe higher concentrations of coastal zooplankton within the core of the eddies, collected by a continuous plankton recorder between 2000 and 2001. Even though the correlation between eddy variability and changes in the ecosystem has not yet been fully established, the ecosystems have been noticed to respond to large-scale atmospheric variability (Mantua et al. 1997; Litzow et al. 2006).

The region is extremely productive at all trophic levels despite observations showing downwelling conditions along the coast (Stabeno et al. 2004), with stronger downwelling condition during winter months. On decadal time scales, the Pacific decadal oscillation (PDO) is the leading mode of North Pacific variability. Changes in the PDO are driven by changes in the Aleutian low pressure system (Figs. 1a,b), which also modulate coastal downwelling conditions. Okkonen et al. (2001) and Combes and Di Lorenzo (2007) show stronger mesoscale eddy activity, during years in which wind forcing

Corresponding author address: Vincent Combes, School of Earth and Atmospheric Sciences, Georgia Institute of Technology, 311 Ferst Drive, Atlanta, GA 30332-0340.
E-mail: vincent.combes@eas.gatech.edu

DOI: 10.1175/2008JPO4014.1

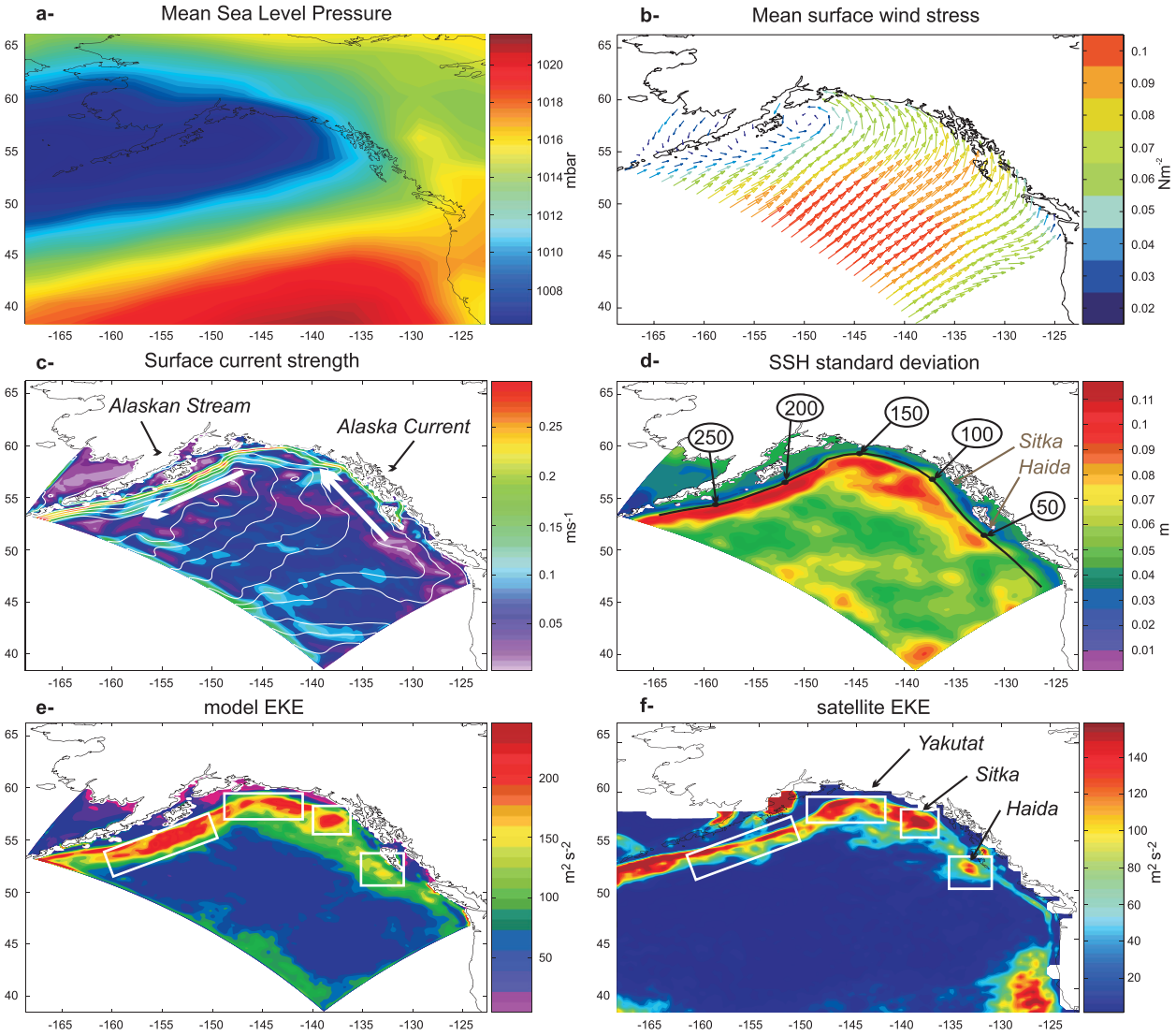

FIG. 1. (a) Mean sea level pressure and (b) mean surface wind stress over the period 1965–2004. (c) Mean surface current strength (m s^{-1}), with mean SSH (white contours), and (d) SSH std dev. (e) Model EKE and (f) AVISO EKE.

promotes strong downwelling. This suggests that interannual and decadal modulations of the GOA open ocean ecosystems may be explained by exploring the statistics of eddy induced cross-shelf transport.

This study investigates the seasonal and interannual variations in cross-shelf transport in the GOA, by looking at the distribution and variability of a passive tracer injected at the coast. The tracer allows us to track coastal water masses and can be used as a proxy for coastal quantities such as iron. The goal of this study is to characterize the statistics of transport of the passive tracer and to understand how changes in atmospheric winds modify the distribution and transport of coastal water masses.

This paper is organized as follows: section 2 describes the model experiment and provides a comparison between model and observational data. Section 3 describes the tracer experiment used in this study. Section 4 discusses the interannual and decadal variations in cross-shelf flux in the eastern (Alaska Current region) and western (Alaskan Stream region) GOA basin. Section 5 provides a summary of the results.

2. Data: Model and observation

The model experiment is performed using the Regional Ocean Modeling System (ROMS; Haidvogel et al. 2008; Shchepetkin and McWilliams 2005). ROMS is a free-surface, hydrostatic, eddy-resolving primitive equation ocean model that uses terrain-following coordinates in the vertical. ROMS has already been used

successfully to study mesoscale processes in the North Pacific (Marchesiello et al. 2003; Di Lorenzo et al. 2005b; Curchitser et al. 2005; Di Lorenzo et al. 2008).

The domain covers the coast from Vancouver Island to the Alaskan Peninsula (Fig. 1c). The grid has an average spatial resolution of ~11 km and uses 42 levels in the vertical, with higher resolution at the upper ocean layer. This resolution is able to capture large eddies in the western and eastern side of the basin, which have an average diameter of 150–200 km (western basin: Crawford et al. 2000; eastern basin: Crawford 2002). The initial conditions and open boundaries are obtained from an outer experiment, which is conducted with the same grid resolution on a larger domain that covers the entire northeast Pacific coast. This outer grid uses boundary conditions from a hindcast simulation using the Community Climate System Model (CCSM; Collins et al. 2006) version of the Parallel Ocean Program (POP; Smith and Gent 2002). The surface forcing functions for the outer experiment (6-hourly forcing at $2^\circ \times 2^\circ$ resolution) are obtained from the Common Ocean-Ice Reference Experiments (CORE), developed by Large and Yeager (2004) and the air–sea fluxes are parameterized using bulk fluxes (Fairall et al. 2003). Our regional nested model uses prescribed surface fluxes obtained by taking the monthly average flux resulting from the outer grid integration. We use the *K*-profile parameterization (KPP) scheme for vertical mixing in the surface boundary (Large et al. 1994) and implicit horizontal mixing associated with the third-order upstream bias scheme (Shchepetkin and McWilliams 1998).

On average, the ocean circulation in the GOA is characterized by a large-scale cyclonic Alaskan gyre, with the broad Alaska Current on the eastern basin and a stronger Alaskan Stream along the Aleutian Islands. The model mean circulation, illustrated in Fig. 1c, is consistent with this view and shows a surface current velocity up to 0.4 m s^{-1} in the western basin associated with a strong cross-shelf sea surface height (SSH) gradient south of the Alaskan Peninsula (white lines in Fig. 1c). Finally, a map of the SSH standard deviation (Fig. 1d) indicates high variability all along the coast, where intense eddy variability is observed (entire basin: Ladd 2007; western basin: Crawford et al. 2000; eastern basin: Tabata 1982; Di Lorenzo et al. 2005a).

To add confidence in the degree of realism of the eddy variability in the model simulation, we compare the model eddy kinetic energy (EKE) to the one derived from the Archiving, Validation, and Interpretation of Satellite Oceanographic data (AVISO) satellite maps (Figs. 1e,f). The satellite EKE is calculated from the sea level anomaly [merged data from the Ocean Topography Experiment (TOPEX)/Poseidon (T/P) or *Jason-1* + *ERS-1/2* and *Envisat* satellites available at http://www.jason.oceanobs.com], as defined by Ladd (2007) by $\mathrm{EKE} = 1/2[\langle U_g'^2 \rangle + \langle V_g'^2 \rangle]$, where U_g' and V_g' are the geostrophic velocity anomalies. Consistent with Ladd (2007), high values of EKE along the Alaska Current (eastern basin) and the Alaskan Stream (western basin) are evident both in the model and the satellite data. On the western GOA basin, eddy activity is constrained to the shelf break. On the eastern GOA basin, we notice the signature of three major eddy groups associated with a region of high EKE, usually named according to the location of their formation: Yakutat, Alaska; Sitka, Alaska; and Haida, Canada (Tabata 1982; Crawford 2002). The eddies observed in the western and eastern basins show different dependencies with the atmospheric forcing reflecting different generation mechanisms. While eddies in the western basin are not directly affected by the atmospheric forcing, the development of mesoscale eddies on the eastern GOA basin is modulated by changes in wind-induced downwelling (Combes and Di Lorenzo 2007; Henson and Thomas 2008) and coastally trapped waves of tropical origin (Melsom et al. 1999). Eddies in the Alaskan Stream (western basin) are often a year or more old when they arrive in this stream, so their strength would also depend mainly on atmospheric conditions when and where they formed.

3. Tracer experiment setup

The transport pathways and statistics associated with the mesoscale circulation in the model are characterized using a passive tracer advection–diffusion equation with a decay term:

$$\frac{\partial P}{\partial t} + \mathbf{u} \cdot \nabla P = A_H \nabla_H^2 P + \frac{\partial}{\partial z}\left(A_V \frac{\partial P}{\partial z}\right) - \frac{P}{\tau} + Q(x, y, z),$$

where P is the passive tracer concentration, A_H is the horizontal diffusivity set to 5 m^2 s^{-1}, A_V is the vertical diffusivity obtained by a KPP scheme (Large et al. 1994), Q is a time-independent source term, and τ is the decay time scale. The source term is such that the passive tracer is set to 1 over a region from the coast to 50 km offshore and from the surface to 50-m depth. The decay term is introduced to track the transport patterns of the passive tracer from its source within the time scale set by τ. This term is needed to avoid an infinite growth of passive tracer concentrations in the model domain interior. The time scale τ is set to 4 yr, which is the average time scale that eddies survive in the gyre after their generation at the coast (Crawford 2002). It also allows the modeled passive tracer to live far longer than iron at the ocean surface. Iron seems mostly to be

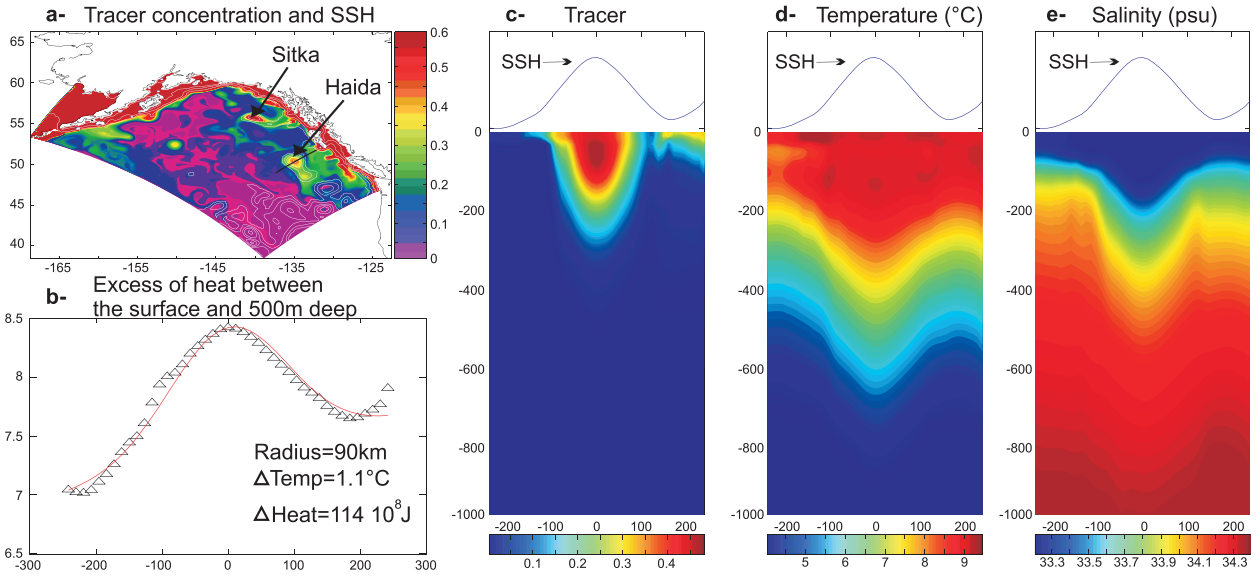

FIG. 2. (a) Tracer concentration and SSH (white contours, contour interval is 5 cm from 0 to 20 cm) for August 1998. (b) The excess of heat across the eddy (the red curve is the fitted Gaussian of the model temperature). Vertical section of (c) tracer, (d) temperature, and (e) salinity.

taken up by phytoplankton in the first spring of an eddy's life (Johnson et al. 2005).

4. Results

We begin by testing if the passive tracer approach realistically tracks the transport of coastal waters associated with eddies generated at the coast. We focus on one model snapshot during August 1998 (Fig. 2a). The eddy field in the eastern basin was dominated by eddies formed during the El Niño of the preceding winter (Melsom et al. 1999; Henson and Thomas 2008), in particular the large anticyclonic Haida and Sitka eddies, which are well reproduced by the model hindcast (white lines in Fig. 2a). The core of the Haida and Sitka eddies corresponds to local maxima in passive tracer concentrations. This confirms that the model adequately reproduces the offshore transport of coastal water, here represented by the passive tracer, within the core of the large-scale eastern basin eddies.

The westward transport associated with the modeled eastern eddies for August 1998 is evident in the vertical section across the Haida eddy core (black transect in Fig. 2a) of tracer concentration (Fig. 2c), temperature (Fig. 2d), and salinity (Fig. 2e). In agreement with observational studies (Crawford 2002; Tabata 1982), Haida eddies (Sitka not shown here) are characterized by an anticyclonic rotation, represented in Fig. 2a by a positive SSH anomaly. These eddies show a warmer and less-saline core than the surrounding water (Figs. 2d,e), with a local maximum in temperature around 100-m depth. The vertical section of the passive tracer (Fig. 2c) shows that the excess of heat and freshwater in the eddy core is advected from the coastal region. This also suggests that other important biochemical quantities can be advected from the coast into the gyre interior, both at the surface and in the subsurface. In the model experiments, the passive tracer is initially set to 1 within a volume that extends 50 km from the coast and 50 m below the surface. Therefore, the presence of a coastal passive tracer (Fig. 2c) below 50 m confirms the results by Combes and Di Lorenzo (2007), who suggest that eastern eddies develop and propagate offshore following a downwelling event at the coast. Finally, Fig. 2b quantifies the excess of heat inside this particular Haida eddy. Identical to Crawford (2005), the excess of heat in the first 500 m is calculated as the excess of heat within a volume associated with a Gaussian function (red fitted curve in Fig. 2b). Consistent with the results of Crawford (2005), the excess of heat is estimated at around 100×10^{18} J between the surface and 500-m depth.

Confident that the model realism is adequate to investigate the cross-shelf transport statistics, we consider the transport of the passive tracer across a transect that follows the coast along the edge of the region of high-SSH standard deviation (black line in Fig. 1d). The cross-shelf exchange across this transect is defined as the advection of the surface passive tracer (P) by the component of the surface velocity normal to the transect (U), where a positive value of the passive tracer flux UP

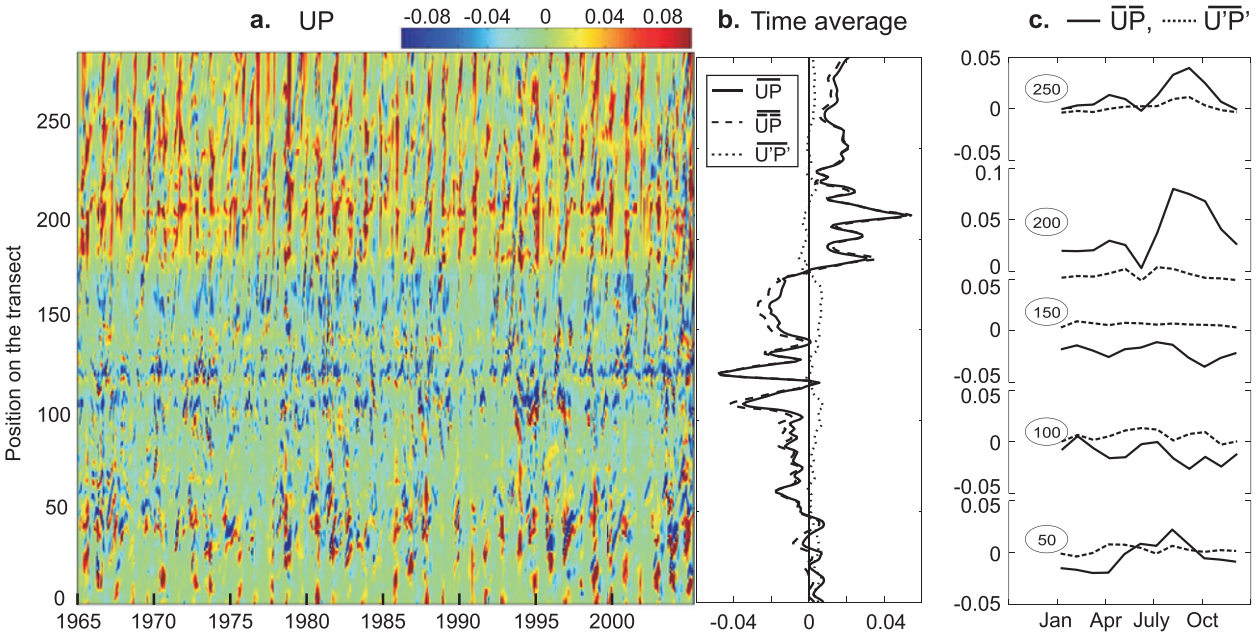

FIG. 3. (a) Hovmöller diagram of the tracer advection (UP) (m s^{-1}). (b) The time average of UP, $\overline{UP}$, and $U'P'$ along the transect. (c) The seasonal variability of $\overline{UP}$ and $\overline{U'P'}$ at locations 50, 100, 150, 200, and 250 on the transect (black line in Fig. 1d).

is directed toward the gyre interior. The temporal evolution of the total surface flux across this transect, as visualized by a Hovmöller diagram from 1965 to 2004 (Fig. 3a), shows significant interannual variability and little spatial coherence along the transect. We now decompose the total flux into

$$UP = \overline{U}\bar{P} + U'\bar{P} + \overline{U}P' + U'P', \qquad (1)$$

where the anomalies (U', P') are defined by removing the monthly cycle (later called "seasonal cycle") $(\bar{U}, \bar{P})$. The time average of the flux terms $\overline{UP} = \overline{\overline{U}\bar{P}} + \overline{U'P'}$ (Fig. 3b) show that the mean total advection at the surface is mainly explained by its seasonal mean $(\overline{\overline{U}\bar{P}})$. Along the eastern basin, the negative value of $\overline{\overline{U}\bar{P}}$ along the transect corresponds to an onshore advection and is consistent with previous papers showing predominant downwelling conditions at the coast. Figure 3b also shows that the mean offshore advection is associated with the mean eddy flux $(\overline{U'P'})$. In the western basin, both the advection of tracers by the average flow and the mean eddy fluxes contribute to the mean offshore advection. The seasonality of $\overline{U}\bar{P}$ and $U'P'$ is illustrated in Fig. 3c at five locations along the transect. The budget of tracer advection integrated over the top 100 m (not shown here) has also been performed and shows similar results.

The spatial patterns of the surface passive tracer seasonal variability can be summarized by the March and September means (Figs. 4a,b). A strong seasonal variability of the surface passive tracer is evident both in the southern edge of the Alaskan Stream and off Vancouver Island, consistent with the advection of tracer across the transect (Fig. 3). South of the Alaskan Peninsula, the surface passive tracer is advected southward with a maximum advection in September. Off Vancouver Island the passive tracer is advected offshore toward the interior of the GOA basin in September (Fig. 4b), whereas in March (Fig. 4a), the surface passive tracer is confined along the coast. The seasonal patterns of the passive tracer closely track the ones observed in satellite chlorophyll-*a* (measured by SeaWiFS satellite; Figs. 4c,d), supporting the hypothesis that offshore transport is the primary mechanism controlling the seasonal chlorophyll maxima in the offshore waters of the GOA (Crawford et al. 2005). It is important to note that Fig. 4 shows a comparison between a surface passive tracer with an active tracer (chlorophyll-*a*), which can explain the difference observed off Vancouver Island.

To explore the interannual variability of the cross-shelf transport, we examine the time series of tracer and tracer flux concentration anomalies, where the anomalies are defined by removing the seasonal cycle $[(UP)_{\text{anomaly}} = U'\bar{P} + \overline{U}P' + (U'P')_{\text{anomaly}}]$. The interannual variability of the flux term (UP anomaly; Fig. 5) shows that the dominant term is anomalous advection acting on the mean tracer concentration ($U'P'$; blue line) with an important contribution also from the eddy

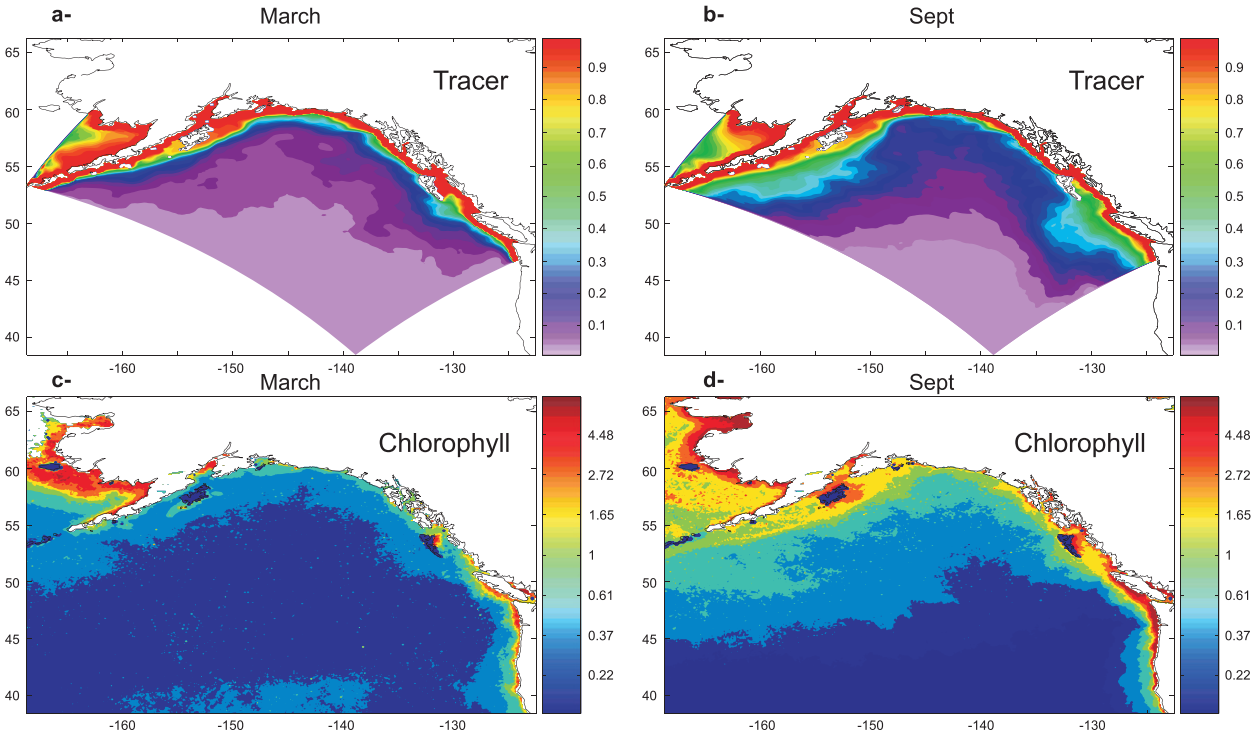

FIG. 4. Surface passive tracer for (a) March and (b) September. Observed surface chlorophyll concentrations (mg m^{-3}) for (c) March and (d) September.

flux anomaly ($U'P'$ anomaly; black line). This result is consistent along all the locations on the transect, both in the eastern (Fig. 5a) and western basins (Fig. 5b). Okkonen et al. (2001) show that eddy variability does not correlate with large-scale atmospheric forcing in the western basin while in the eastern basin eddy variability is modulated by changes in the surface winds. In particular, Okkonen et al. (2001) and Combes and Di Lorenzo

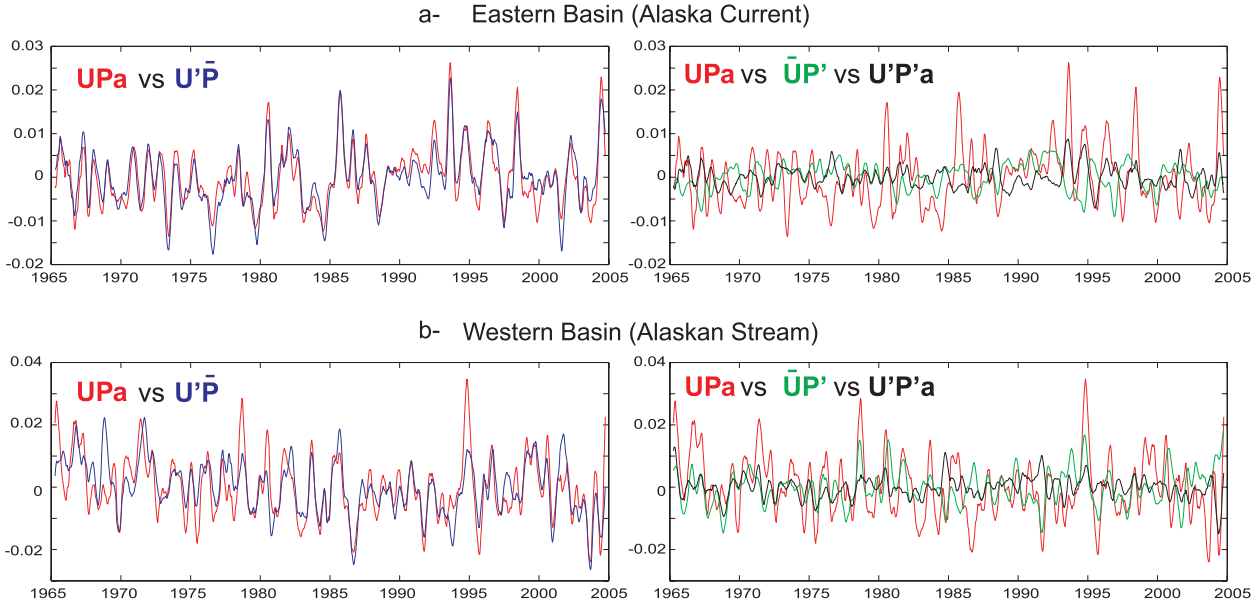

FIG. 5. Components of *UP* anomaly (UPa; red line) along the (a) Alaska Current and (b) Alaskan Stream.

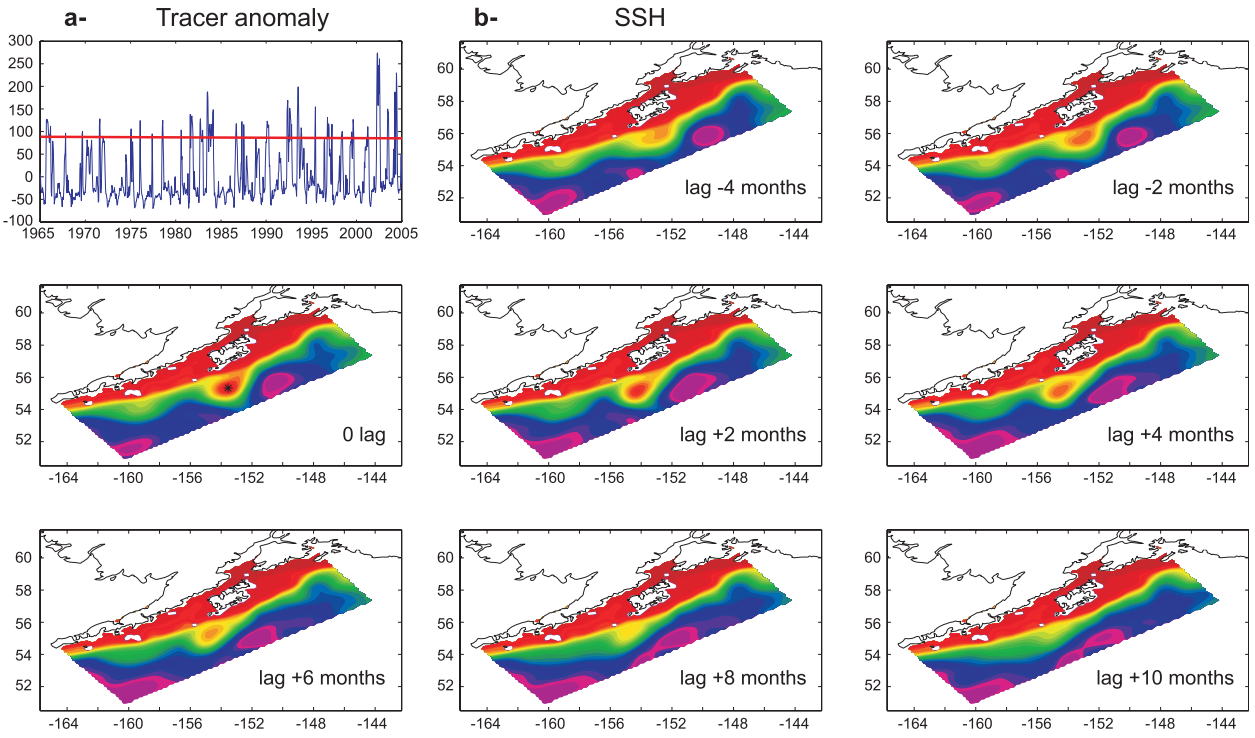

FIG. 6. (a) Tracer concentration anomaly at (55.11°N, 153.28°W) [black star in (b)]. (b) SSH composite maps for tracer anomaly > 90 [red line in (a)].

(2007) show strong mesoscale eddy activity in the eastern basin during years in which wind forcing promotes strong downwelling. When discussing eddy transport, it is better to use the depth-integrated passive tracer rather than a tracer concentration at the surface or at a certain depth. From now on, ''tracer'' will refer to the depth-integrated tracer over the entire water column.

We first explore regions of high-SSH standard deviation in the western basin. Figure 6a shows the time series of tracer anomaly for the location represented by a black star in Fig. 6b lag 0 (55.11°N, 153.28°W) from 1965 to 2004 and exhibits a strong interannual variability. Figure 6b (lag 0) shows a composite analysis of the SSH during times when the depth-integrated tracer concentration anomalies at (55.11°N, 153.28°W) are greater than 90 (red line in Fig. 6a). The sequence of maps of SSH at different lags with respect to the time when the tracer anomaly is high shows the formation and propagation of an anticyclonic eddylike feature, implying that the high anomalous coastal passive tracer found along the western basin is mainly associated with eddy variability. These types of features are found all along the western basin and advect coastal water, both in their center and periphery, along the Alaskan Stream.

Previous studies have suggested that variability in oceanic circulation and eddies generated on the eastern GOA is modulated by changes in the wind stress (Melsom et al. 1999; Combes and Di Lorenzo 2007). On a decadal time scale, along the Alaska Current, changes in wind stress are associated with changes in the PDO index. The PDO index is negative from 1950 to 1976 and principally positive from 1977 to 2000. The positive phase of the PDO is associated with an enhancement of the Aleutian low pressure system over the North Pacific.

To establish the link between the different phases of the PDO and offshore transport, the changes in tracer concentration are computed as the difference between the passive tracer distribution in the period 1977–82 and in the period 1971–76. The eastern GOA shows a significant change in tracer distribution following the 1976–77 climate shift (Fig. 7a). Figure 7a shows an increase of passive tracer advection to the interior of the gyre when the Aleutian low pressure is strengthening. The advection is more pronounced west of the Sitka region and west of Queen Charlotte Island, where the Sitka and Haida eddies are generated. Changes in atmospheric forcing also produce a change of the surface coastal current. An intensification of the surface current is found in the eastern basin, associated with the 1976–77 climate shift, leading to a stronger passive tracer advection. In contrast to the western basin, interannual variability in the tracer concentration (shown previously) does

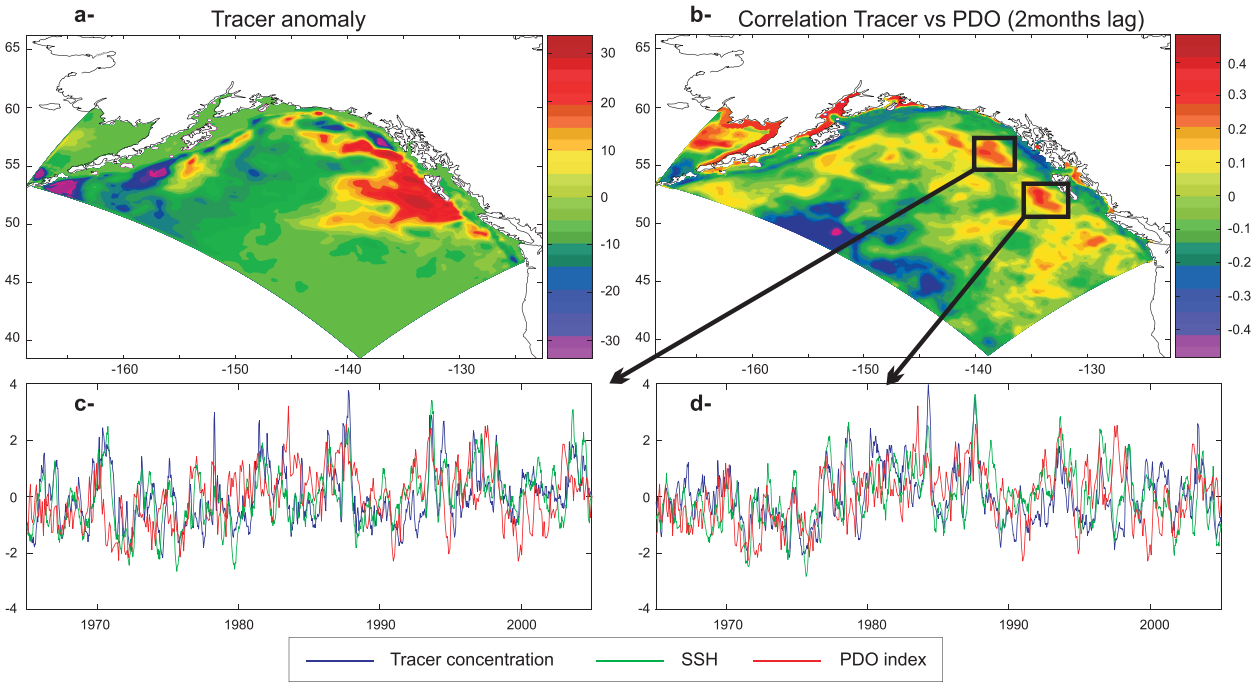

FIG. 7. (a) Tracer distribution associated with the 1976–77 climate shift. (b) The correlation between the PDO index and tracer concentration (lag 2 months). Comparison between the tracer (blue), SSH (green), and PDO index (red) at (c) Sitka and (d) Haïda.

not seem to respond to changes of surface forcing associated with the climate shift.

To further clarify the relationship between tracer distribution and PDO, we quantify the PDO effect by correlating the tracer concentration with the PDO index (Fig. 7b). Figure 7b shows the spatial distribution of tracer 2 months after the PDO affects the ocean surface. The map shows principally two regions of high correlation between the tracer and PDO. These regions are located on the path of the Haida and Sitka eddies, which advect the passive tracer trapped in their core. This is also evident in time series of SSH, tracer concentration along the path of the Haida and Sitka eddies, and the PDO index (Figs. 7c,d). These results corroborate the hypothesis that the PDO explains much of the decadal variability of the tracer concentration in the eastern basin, and suggest an increase in the mean offshore transport from the eastern coast after the 1976–77 climate shift. The weaker correlation between tracer concentration and PDO time series, observed in Figs. 7c and 7d after 1998, may be due to the dominance in recent decades of the second mode of variability, known as the Victoria (Bond et al. 2003) or the North Pacific gyre oscillation (NPGO) mode (Di Lorenzo et al. 2008).

5. Conclusions

The passive tracer simulation, analyzed in this study, provides a method to explore the evolution and distribution of coastal water masses into the gyre interior. The general features of the model circulation of the GOA show consistent results with observational data; in particular, both model and satellite data reveal high-EKE regions in the western basin, the northern Gulf of Alaska, and the eastern basin where the anticyclonic Haida and Sitka eddies develop. Throughout the coastal Gulf of Alaska, the presence of passive tracer within the core of the anticyclonic eddies confirms that eddies advect coastal waters into the gyre interior. This result implies that, in addition to warm and freshwater, eddies also transport oxygen-poor water and important biochemical quantities such as chlorophyll-*a* (Crawford et al. 2005), nutrients, and micronutrients (e.g., iron), essential for productivity. Along the eastern side of the GOA basin north of Vancouver Island, the passive tracer analysis shows on average that while the advection of tracers by the average flow at the surface is directed toward the coast, consistent with the dominant downwelling regime of the GOA, it is the mean eddy fluxes that contribute to offshore advection into the gyre interior. In the western basin, both the advection of tracers by the average flow and the mean eddy fluxes contribute to the mean offshore advection. The passive tracer distribution in the GOA also exhibits a strong seasonal variability both in the eastern and western basin. On the seasonal time scales, passive tracer is clearly advected toward the interior of the gyre in September.

Significant tracer is transported westward, off Vancouver Island (eastern basin), and southward, south of the Alaskan Peninsula (western basin).

On interannual time scales, the cross-shelf transport in the western region (along the Alaskan Stream) is mainly associated with intrinsic eddy variability. In contrast, along the eastern boundary in the Alaska Current region, stronger offshore transport of the passive tracer coincides with periods of stronger downwelling conditions, which trigger the development of stronger eddies. For instance, after the 1976–77 climate shift when the Aleutian low pressure intensifies and stronger coastal downwelling conditions become predominant throughout the GOA, stronger advection of coastal passive tracer is found in the eastern basin (Fig. 6a), in particular in the path of coastal eastern eddies, such as the Haida and Sitka eddies.

Our results indicate that coastal water, and therefore biochemical quantities, are advected both vertically (upwelling and downwelling) and horizontally (advection by surface current or eddies) in the Gulf of Alaska. The cross-shelf and vertical transports are essential for the productivity in the basin. The relation between eddy transport and biota has already been observed in the western basin (Okkonen et al. 2003) and eastern basin (Mackas and Galbraith 2002). Therefore the increase in cross-shelf transport after the 1976–77 climate shift may provide an additional mechanism to explain shifts in species distribution and fish abundance (Mantua et al. 1997; Litzow et al. 2006).

Acknowledgments. The research was supported by funding from NSF OCE-0550266, NSF GLOBEC OCE-0606575, NASA OES-NNG05GC98G, and NSF OCE-0452654. We thank the two anonymous reviewers who helped improve the manuscript considerably. We also acknowledge the support from the Pacific Boundary Ecosystem and Climate project sponsored by NSF GLOBEC OCE-0815280.

REFERENCES

Batten, S. D., and W. R. Crawford, 2005: The influence of coastal origin eddies on oceanic plankton distributions in the eastern Gulf of Alaska. *Deep-Sea Res. II,* **52,** 991–1009.

Bond, N. A., J. E. Overland, M. Spillane, and P. Stabeno, 2003: Recent shifts in the state of the North Pacific. *Geophys. Res. Lett.,* **30,** 2183, doi:10.1029/2003GL018597.

Boyd, P. W., and Coauthors, 2004: The decline and fate of an iron-induced subarctic phytoplankton bloom. *Nature,* **428,** 549–553.

Collins, W. D., and Coauthors, 2006: The Community Climate System Model version 3 (CCSM3). *J. Climate,* **19,** 2122–2143.

Combes, V., and E. Di Lorenzo, 2007: Intrinsic and forced interannual variability of the Gulf of Alaska mesoscale circulation. *Prog. Oceanogr.,* **75,** 266–286.

Crawford, W. R., 2002: Physical characteristics of Haida Eddies. *J. Oceanogr.,* **58,** 703–713.

——, 2005: Heat and fresh water transport by eddies into the Gulf of Alaska. *Deep-Sea Res. II,* **52,** 893–908.

——, J. Y. Cherniawsky, and M. G. G. Foreman, 2000: Multi-year meanders and eddies in the Alaskan Stream as observed by TOPEX/Poseidon altimeter. *Geophys. Res. Lett.,* **27,** 1025–1028.

——, P. J. Brickley, T. D. Peterson, and A. C. Thomas, 2005: Impact of Haida Eddies on chlorophyll distribution in the eastern Gulf of Alaska. *Deep-Sea Res. II,* **52,** 975–989.

Curchitser, E. N., D. B. Haidvogel, A. J. Hermann, E. L. Dobbins, T. M. Powell, and A. Kaplan, 2005: Multi-scale modeling of the North Pacific Ocean: Assessment and analysis of simulated basin-scale variability (1996–2003). *J. Geophys. Res.,* **110,** C11021, doi:10.1029/2005JC002902.

Di Lorenzo, E., M. G. G. Foreman, and W. R. Crawford, 2005a: Modelling the generation of Haida Eddies. *Deep-Sea Res. II,* **52,** 853–873.

——, A. J. Miller, N. Schneider, and J. C. McWilliams, 2005b: The warming of the California current system: Dynamics and ecosystem implications. *J. Phys. Oceanogr.,* **35,** 336–362.

——, and Coauthors, 2008: North Pacific Gyre Oscillation links ocean climate and ecosystem change. *Geophys. Res. Lett.,* **35,** L08607, doi:10.1029/2007GL032838.

Fairall, C. W., E. F. Bradley, J. E. Hare, A. A. Grachev, and J. B. Edson, 2003: Bulk parameterization of air–sea fluxes: Updates and verification for the COARE algorithm. *J. Climate,* **16,** 571–591.

Haidvogel, D., and Coauthors, 2008: Ocean forecasting in terrain-following coordinates: Formulation and skill assessment of the Regional Ocean Modeling System. *J. Comput. Phys.,* **227,** 3595–3624.

Harrison, P. J., P. W. Boyd, D. E. Varela, and S. Takeda, 1999: Comparison of factors controlling phytoplankton productivity in the NE and NW subarctic Pacific gyres. *Prog. Oceanogr.,* **43,** 205–234.

Henson, S. A., and A. C. Thomas, 2008: A census of oceanic anticyclonic eddies in the Gulf of Alaska. *Deep-Sea Res. I,* **55,** 163–176.

Johnson, W. K., L. A. Miller, N. E. Sutherland, and C. S. Wong, 2005: Iron transport by mesoscale Haida eddies in the Gulf of Alaska. *Deep-Sea Res. II,* **52,** 933–953.

Ladd, C., 2007: Interannual variability of the Gulf of Alaska eddy field. *Geophys. Res. Lett.,* **34,** L11605, doi:10.1029/2007GL029478.

——, P. Stabeno, and E. D. Cokelet, 2005: A note on cross-shelf exchange in the northern Gulf of Alaska. *Deep-Sea Res. II,* **52,** 667–679.

Large, W., and S. Yeager, 2004: Diurnal to decadal global forcing for ocean and sea-ice models: The data sets and flux climatologies. NCAR Tech. Note NCAR/TN-460+1STR, CGD Division of the National Center for Atmospheric Research.

Large, W. G., J. C. McWilliams, and S. C. Doney, 1994: Oceanic vertical mixing: A review and a model with a nonlocal boundary layer parameterization. *Rev. Geophys.,* **32,** 363–403.

Litzow, M. A., K. M. Bailey, F. G. Prahl, and R. Heintz, 2006: Climate regime shifts and reorganization of fish communities: The essential fatty acid limitation hypothesis. *Mar. Ecol. Prog. Ser.,* **315,** 1–11.

Mackas, D. L., and M. D. Galbraith, 2002: Zooplankton distribution and dynamics in a North Pacific eddy of coastal origin: 1. Transport and loss of continental margin species. *J. Oceanogr.,* **58,** 725–738.

Mantua, N. J., S. R. Hare, Y. Zhang, J. M. Wallace, and R. C. Francis, 1997: A Pacific interdecadal climate oscillation with

impacts on salmon production. *Bull. Amer. Meteor. Soc.,* **78,** 1069–1079.

Marchesiello, P., J. C. McWilliams, and A. Shchepetkin, 2003: Equilibrium structure and dynamics of the California Current System. *J. Phys. Oceanogr.,* **33,** 753–783.

Melsom, A., S. D. Meyers, H. E. Hurlburt, E. J. Metzger, and J. J. O'Brien, 1999: ENSO effects on Gulf of Alaska eddies. *Earth Interactions,* **3.** [Available online at http://earthinteractions.org/.]

Okkonen, S. R., G. A. Jacobs, E. J. Metzger, H. E. Hurlburt, and J. F. Shriver, 2001: Mesoscale variability in the boundary currents of the Alaska Gyre. *Cont. Shelf Res.,* **21,** 1219–1236.

——, T. J. Weingartner, S. L. Danielson, D. L. Musgrave, and G. M. Schmidt, 2003: Satellite and hydrographic observations of eddy-induced shelf-slope exchange in the northwestern Gulf of Alaska. *J. Geophys. Res.,* **108,** 3033, doi:10.1029/2002JC001342.

Shchepetkin, A., and J. C. McWilliams, 1998: Quasi-monotone advection schemes based on explicit locally adaptive dissipation. *Mon. Wea. Rev.,* **126,** 1541–1580.

——, and ——, 2005: The Regional Oceanic Modeling System (ROMS): A split-explicit, free-surface, topography-following-coordinate oceanic model. *Ocean Modell.,* **9,** 347–404.

Smith, R. D., and P. R. Gent, 2002: Reference manual for the Parallel Ocean Program (POP), ocean component of the Community Climate System Model (CCSM2.0 and 3.0).Tech. Rep. LA-UR-02-2484, Los Alamos National Laboratory. [Available online at http://www.ccsm.ucar.edu/models/ccsm3.0/pop.]

Stabeno, P. J., N. A. Bond, A. J. Hermann, N. B. Kachel, C. W. Mordy, and J. E. Overland, 2004: Meteorology and oceanography of the Northern Gulf of Alaska. *Cont. Shelf Res.,* **24,** 859–897.

Tabata, S., 1982: The anticyclonic, baroclinic eddy off Sitka, Alaska, in the northeast Pacific Ocean. *J. Phys. Oceanogr.,* **12,** 1260–1282.

Whitney, F., and M. Robert, 2002: Structure of Haida eddies and their transport of nutrient from coastal margins into the NE Pacific Ocean. *J. Oceanogr.,* **58,** 715–723.